

# A mechanism for brief glacial episodes in the Mesozoic greenhouse

Yannick Donnadieu,<sup>1</sup> Gilles Dromart,<sup>2</sup> Yves Godd  ris,<sup>3</sup> Emmanuelle Puc  at,<sup>4</sup>  
Benjamin Brigaud,<sup>5</sup> Guillaume Dera,<sup>1</sup> Christophe Dumas,<sup>1</sup> and Nicolas Olivier<sup>2</sup>

Received 9 December 2010; revised 25 March 2011; accepted 9 May 2011; published 17 August 2011.

[1] The Mesozoic, perhaps the longest period of warmth during the Phanerozoic Earth history, has been repeatedly affected by short-lived cold interludes lasting about one million years. While the origin of these cold snaps has been classically attributed to a temporary atmospheric CO<sub>2</sub> drawdown, quantified mechanisms explaining these instabilities of the carbon cycle are still lacking. Based on a climate carbon cycle model, we show that the general demise of carbonate platforms accompanying these short-lived cold interludes is a powerful mechanism capable of generating a fast atmospheric CO<sub>2</sub> decrease and a moderate sea level drop associated with ice sheet buildup. The temporary nature of the carbonate production decline explains the relative short time of these cold events but makes it possible to account for ice sheet waxing and waning.

**Citation:** Donnadieu, Y., G. Dromart, Y. Godd  ris, E. Puc  at, B. Brigaud, G. Dera, C. Dumas, and N. Olivier (2011), A mechanism for brief glacial episodes in the Mesozoic greenhouse, *Paleoceanography*, 26, PA3212, doi:10.1029/2010PA002100.

## 1. Introduction

[2] Transitions from greenhouse to icehouse conditions have been intensively studied, particularly with the renewed interest in the conditions leading to the Neoproterozoic glaciations [Hoffman *et al.*, 1998] as well as for those triggering the inception of ice sheets over Gondwana during the Permo-Carboniferous [Horton *et al.*, 2007] and over Antarctica across the Eocene-Oligocene boundary [Coxall *et al.*, 2005; DeConto and Pollard, 2003; Merico *et al.*, 2008]. Although the state of the Earth system is very different for each ice age, atmospheric CO<sub>2</sub> level drawdown is commonly required to explain the long-term general cooling trend to initiate glaciation. Transitions from a high CO<sub>2</sub> world to a low CO<sub>2</sub> world are often ascribed to a permanent increase in silicate weathering resulting, for example, from the breakup of the Rodinia supercontinent for the Neoproterozoic cool period [Donnadieu *et al.*, 2004] or from the widespread appearance of land plants for the Permo-Carboniferous cool period [Berner, 1997]. Mesozoic cold interludes are completely at odds with classical ice age theory because they are not associated with any long-term global cooling trend and last for about one million years [Dromart *et al.*, 2003b; McArthur *et al.*, 2007; Steuber *et al.*, 2005]. These events challenge our knowledge of the Earth system because they require the identification of non-permanent processes capable of triggering climatic cooling for a short time period.

[3] In this contribution, we focus on the Middle Late Jurassic Transition (MLJT) about 160 Ma ago [Dromart *et al.*, 2003a]. A short-lived drop in seawater temperature around the Callovian-Oxfordian transition has been identified using the oxygen isotope composition of shark tooth enamel, belemnite rostra and bivalve shells from Tethyan and sub-Arctic domains [Dromart *et al.*, 2003b; Brigaud *et al.*, 2009; Price and Rogov, 2009; Nunn and Price, 2010]. Although the influence of local paleoceanic changes implying cool water influxes cannot be completely excluded [Wierzbowski and Rogov, 2011], other independent proxies support the climatic interpretation for a cooling trend: (1) palynological and clay mineral data indicating that continental air became markedly cooler in north Europe hinterlands [Abbink *et al.*, 2001; Pellenard and Deconinck, 2006], (2) successive southward invasions of boreal ammonite families in the NW Tethyan domains [Thierry *et al.*, 2006] and (3) a local CO<sub>2</sub> minimum [Royer *et al.*, 2004] located at the MLJT in the proxy record of CO<sub>2</sub>. During the Callovian and Oxfordian periods, perturbations in the carbonate deposition pattern occur [Dromart *et al.*, 2003a] as evidenced by shrinkage of the latitudinal extent of carbonate platforms followed by a general demise of carbonate platforms deposition. By the end of the Early Callovian, carbonate platform deposition had ceased on the midlatitude platforms located above 25   (i.e., West Europe and East Africa) and was confined to low latitudes. Finally, low-latitude platforms experienced a short shutdown of production in the latest Callovian, correlative in time with the cooling.

[4] Here, we investigate the climate-carbon cycle behavior during the Middle-Late Jurassic Transition using a general circulation model with coupled components for atmosphere, ocean, cryosphere and biogeochemical cycles of C, O and P [Donnadieu *et al.*, 2006]. We force our climate-carbon model

<sup>1</sup>LSCE, IPSL, CEA-CNRS-UVSQ, Gif-sur-Yvette, France.

<sup>2</sup>UMR 5570, Universit   de Lyon, CNRS, ENS de Lyon, France.

<sup>3</sup>LMTG, CNRS-Universit   Paul Sabatier, Toulouse, France.

<sup>4</sup>Universit   de Bourgogne, CNRS Biog  osciences, Dijon, France.

<sup>5</sup>UMR 8148, Universit   Paris-Sud 11, CNRS, Orsay, France.

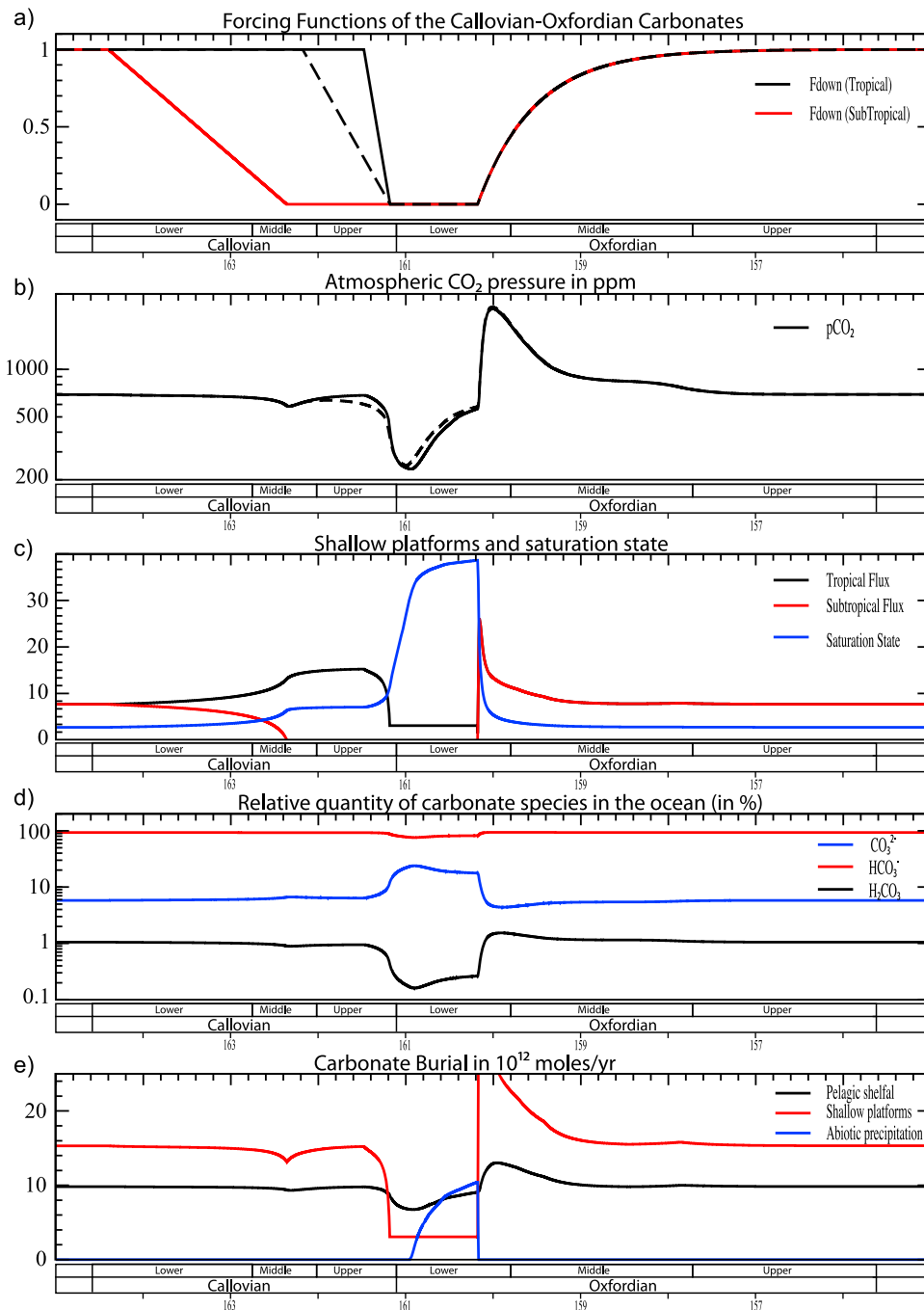


**Figure 1.** Model results simulating the effects of the collapse and the recovery of the carbonate platforms during the Middle Late Jurassic transition. (a) Fdown function as described in the main text. (b) Changes in atmospheric CO<sub>2</sub> content. Note that the first collapse is more diluted in times than the second one based on geological data. Nevertheless, the effect remains the same when increasing the time for the collapse (see dashed curve). (c) Changes in the burial flux coming from tropical and subtropical platforms. Note the remaining flux of the tropical shallow carbonate platform during the crisis (i.e., 20% here). We have also plotted the mean saturation state. (d) Distribution of the carbonate species. (e) Changes in sedimentary calcium carbonate burial fluxes. The black curve represents the neritic platform carbonate burial flux, the red curve represents the pelagic shelfal carbonate burial, and the green curve represents “abiotic” carbonate production flux (see text). Note that the neritic/global carbonate production ratio is 65% in this run. Platform collapse lasts for 1 million years; 20% of the preperiturbation platform burial flux is conserved during the crisis in order to account for the likely possibility that carbonate platforms still exist in specific environments.

with geological evidence of the evolution of carbonate production in the mid and low latitudes [Dromart *et al.*, 2003a, 2003b].

## 2. Methods

### 2.1. General Settings

[5] To test the influence of these perturbations in the carbonate factory on atmospheric CO<sub>2</sub> and climate, we carried out a suite of simulations with the GEOCLIM model [Donnadieu *et al.*, 2006, 2009; Godderis *et al.*, 2008]. The numerical model GEOCLIM couples a 3D general circulation model (FOAM) to a model of the biogeochemical cycles of carbon, alkalinity, oxygen and phosphate (COMBINE) (see Donnadieu *et al.* [2006] for a full description). The COMBINE model has been upgraded since its original version [Godderis and Joachimski, 2004]. The geometry of the ocean has been changed, and the model now includes 9 oceanic boxes divided into, 2 high-latitude oceans (each including a photic zone and a deep ocean reservoirs), a low- to middle-latitude ocean (with a photic zone, thermocline and deep oceanic reservoirs) and an epicontinental sea (with a photic zone and a deep epicontinental reservoirs), and one box for the atmosphere. Exchange water fluxes between boxes are tuned to fit the present-day vertical distribution of the oxygen, DIC and alkalinity in the low-to-middle-latitude ocean. The atmospheric component of FOAM is a parallelized version of NCAR's Community Climate Model 2 (CCM2) with the upgraded radiative and hydrologic physics incorporated in CCM3 v. 3.2. The atmosphere runs at R15 spectral resolution ( $4.5^\circ \times 7.5^\circ$ ) with 18 levels. We use FOAM in mixed-layer mode, i.e., the atmospheric model is linked to a 50 m mixed-layer ocean, which parameterizes heat transport through diffusion, mainly for computation time considerations. A full coupling between COMBINE and FOAM cannot be achieved owing to excessive computation times. Hence we adopt an indirect coupling that employs lookup tables from a catalog of simulations. For a given paleogeography we run a suite of FOAM experiments (30 years for each to reach the steady state) in which the only factor that varies is atmospheric CO<sub>2</sub>. Atmospheric CO<sub>2</sub> is tested over a range from 4200 to 200 ppm, which covers all plausible atmospheric CO<sub>2</sub> content for the Mesozoic time period. We linearly interpolate between experiments to obtain climatic variables (temperature and runoff) for any CO<sub>2</sub> value within our CO<sub>2</sub> range. These climatic parameters allow the calculation of the weathering rates within the 1920 grid elements using weathering laws linking climatic factors (temperature and runoff) to CO<sub>2</sub> consumption through silicate weathering. We want to emphasize here that phosphorus flux from the continents are also calculated through the climatic dependency of the continental weathering. Fixing the CO<sub>2</sub> degassing to a given constant value, the numerical feedback loop between FOAM and COMBINE is run until a steady state PCO<sub>2</sub> is reached. Each continental configuration is thus finally characterized by a steady state atmospheric PCO<sub>2</sub>. The MLJT land-ocean distribution used here is derived from a synthesis of paleomagnetic data, hot spot tracks and geologic constraints [Besse and Courtillot, 2002; Dercourt *et al.*, 1993]. Surface types are set to average model surface characteristics (i.e., deciduous forest) and the Earth's orbit around the Sun is circular (eccentricity = 0) and the Earth's obliquity is  $23.5^\circ$  (this setting leads to an equal annual insolation for both hemi-

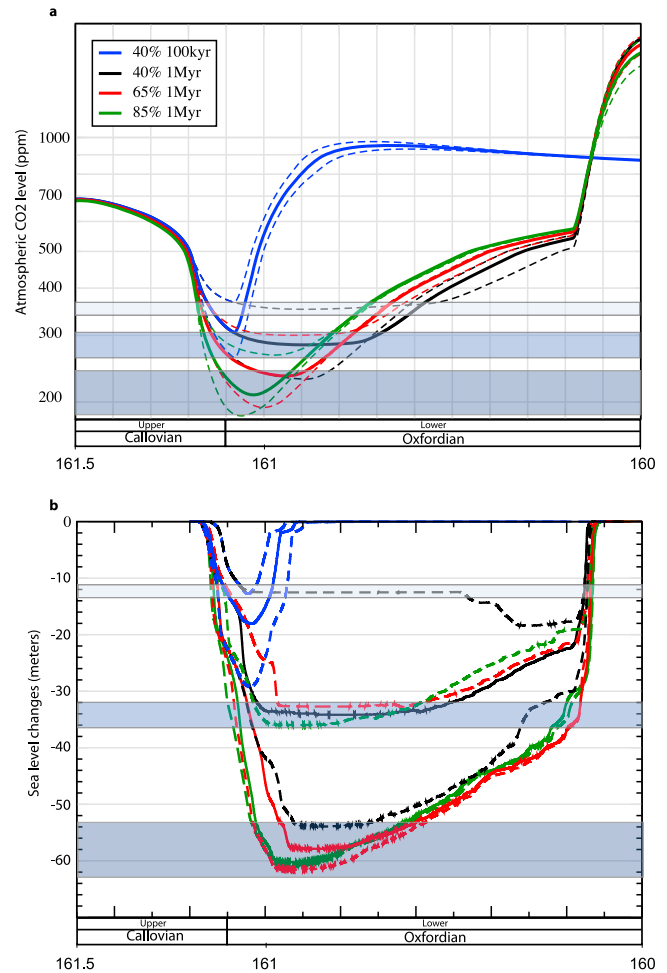


**Figure 2.** Sensitivity of CO<sub>2</sub> and induced sea level fall. (a) Atmospheric CO<sub>2</sub> simulated in GEOCLIM zoomed on the 3.5–5 Ma period corresponding to the Middle Late Jurassic Transition. Black, red, and green solid lines represent results for a percentage of total carbonate burial originating from neritic platform like producers being 40, 65, and 85%, respectively. Twenty percent of the pre-perturbation carbonate platform burial flux is conserved during the crisis for these runs. Top and bottom dashed lines of the same color represent runs in which 40 and 0% of the pre-perturbation carbonate platform burial flux is conserved during the crisis. Blue lines come from a run in which settings are the same as those from the red lines except the duration of the crisis that is diminished to last 100 kyr. (b) Sea level fall simulated using the GRIZZLI model forced by GEOCLIM output. Color codes remain the same as those described in Figure 2a. Blue areas denote CO<sub>2</sub> ranges for which the sea level fall is found to be around 12, 34, and 58 m.

spheres). Solar luminosity is assumed to evolve through time according to the stellar evolution models [Gough, 1981]. As described by Donnadieu *et al.* [2006], the long-term steady state atmospheric CO<sub>2</sub> level characterizing the Middle Jurassic paleogeography is 700 ppm (see Figure 1 also). In other words, 700 ppmv of CO<sub>2</sub> are required in the Middle Jurassic for the calculated silicate weathering to balance the prescribed solid Earth degassing. Note that because there is no consensus about the Earth degassing rate for the last 200 million years, we choose to keep it constant at its present-day value, assuming

the present-day equality between  $\text{CO}_2$  consumption by continental silicate rock weathering ( $6.8 \times 10^{12}$  moles  $\text{CO}_2/\text{yr}$  today [Gaillardet *et al.*, 1999]) and  $\text{CO}_2$  degassing. In contrast to previous investigations of the past climatic and geochemical evolution of the Earth system with the GEOCLIM model, GEOCLIM is run dynamically in this study. This means that the long-term steady state of the carbon cycle, requiring the close balance between silicate weathering and solid Earth degassing, is not prescribed. Over the course of the simulation, and depending on the dynamics of the alkalinity, and organic and inorganic carbon cycles, significant departures between silicate weathering and solid Earth degassing are calculated [Walker *et al.*, 1981].

[6] We use the GRISLI ice sheet model (ISM) to reconstruct ice sheet topography during the MLJT. GRISLI simulates the dynamics of grounded ice as well as ice shelves and ice stream regions. Inland ice deforms according to the stress balance using the shallow-ice approximation. Ice shelves and dragging ice shelves (ice streams) are described following MacAyeal [1989]. This 3-D model has been developed and validated over Antarctica by Ritz *et al.* [2001]. Ritz *et al.* [2001] provide a comprehensive description of the model. Three data sets are used from the FOAM simulations as the input to the GRISLI model: surface temperature from the hottest month, mean annual temperature and mean annual precipitation (i.e., snow and rain). The climatological variables are interpolated to the fine grid topography of the ISM using constant lapse-rate corrections (for the temperature) and an exponential law (for the precipitation). The first two of these data sets are used to compute ablation at the ice sheet surface, and the last two to compute accumulation. Therefore, the feedback of the ice on the GCM-simulated climate is not taken into account but the lapse-rate corrections still capture much of the interactions. GEOCLIM provides time evolution of atmospheric  $\text{CO}_2$  and climate during the Middle Late Jurassic Transition. These scenarios are then used to force the GRISLI model (Figure 2).

## 2.2. Forcing the Carbonate Factory to Decline

[7] The simulations performed in this study require imposing a perturbation of the oceanic inorganic carbon cycle through a change in carbonate deposition rates. In GEOCLIM, seawater carbonate speciation is explicitly resolved in every oceanic reservoir at each time step from the budget equations for DIC and alkalinity. This includes the calculation of the  $\text{H}_2\text{CO}_3$ ,  $\text{HCO}_3^-$ , and  $\text{CO}_3^{2-}$  concentrations in each oceanic reservoir over the course of the simulation. In the previously published version of GEOCLIM, carbonate production occurs through (1) shallow carbonate platforms and (2) planktonic organisms. Carbonate production on platforms is expressed in the model as a proportionality with  $(\Omega-1)^n$ , where  $\Omega$  is defined as  $([\text{Ca}^{2+}] \times [\text{CO}_3^{2-}])/K_s$  (where  $K_s$  is the calcium carbonate solubility product, itself dependent on pressure and temperature). The kinetic parameter,  $n$  reflects how the carbonate precipitation rate changes in response to a change in ambient  $[\text{Ca}^{2+}]$  or  $[\text{CO}_3^{2-}]$ : a value of 1.7 is commonly assumed [Caldeira and Rampino, 1993]. Planktonic carbonate production is dependent on the primary productivity (linked to the phosphorus upwelling flux) and on the saturation state of the water through a relationship calculating the PIC/POC ratio [Gehlen *et al.*, 2007].

[8] In summary, carbonate production is a function of the saturation state of seawater and of the primary organic productivity. The temperature dependency appears in the term  $K_s$ . These formulations may seem overly simple but, to our knowledge, no more complex formulations currently exist even in present-day modeling studies of the carbonate production [Orr *et al.*, 2005]. In addition, using the PaleoReef database, Kiessling [2001] showed that the link between the paleoclimatic evolution of the Earth and the latitudinal extension of carbonate reefs was not statistically significant. Neither the width of the tropical reef zone nor the total latitudinal range of reefs is correlated with published estimates of paleotemperature. As a consequence, we restrict ourselves in this paper to the study of the effect of carbonate production decrease on the carbon cycle and on climate in terms of feedbacks. Nevertheless, possible (including climatic) causes of the carbonate production decrease at the MLJT will be tentatively discussed in section 4.

[9] In order to quantify the consequences of the decline of shallow carbonate platform growth occurring at the LMJT on the carbon cycle and on climate, the GEOCLIM model has been modified to divide the original epicontinental reservoir where shallow carbonate platforms are assumed to occur into two different epicontinental seawater reservoirs: one for the tropical latitude (below  $30^\circ$  lat), and one for the subtropical latitudes. Indeed, as defined by Dromart *et al.* [2003a], three stages have been distinguished in global carbonate sedimentation around the MLJT: (1) for the latest Bathonian to Middle Callovian, a withdrawal by drowning of shallow carbonate platforms from subtropical latitudes; (2) for the latest Callovian to Early Oxfordian, a widespread and pronounced decline of the carbonate sedimentation from the tropical latitudes; and (3) during the Middle Oxfordian, a general and abrupt recovery of carbonate platforms to preevent ranges and accumulation rates.

[10] Because we cannot explicitly model the demise of the carbonate platform in GEOCLIM, we have introduced a dimensionless parameter called  $f_{\text{down}}$ . Two  $f_{\text{down}}$  parameters are defined: one for the shallow carbonate platforms from subtropical latitudes, and the second for the shallow carbonate platforms from tropical latitudes.  $f_{\text{down}}$  varies between 1 and 0 (see Figure 1a). This parameter allows us to force the collapse of the subtropical carbonate platforms slowly and the collapse of the tropical platforms more rapidly (Figures 1a and 1c). The carbonate burial flux due to the shallow carbonate platform is then expressed as follows:

$$F_{\text{neritic}}^i = k_{\text{neritic}} (\Omega^i - 1)^n f_{\text{down}}^i$$

The index  $i$  makes it possible to distinguish subtropical and tropical shallow carbonate platforms.  $k_{\text{neritic}}$  is a proportionality constant calibrated so that the present-day shallow carbonate deposition reaches  $22 \times 10^{12}$  mol/yr under present-day conditions (about 2/3 of the global carbonate accumulation) [Catubig *et al.*, 1998]. It is important to note that neritic carbonate deposition is not completely forced. The saturation factor  $(\Omega-1)^n$  still allows neritic carbonate deposition to respond to changes in the environmental conditions.

## 2.3. Deep Times Uncertainties

[11] Our aim is to force the carbonate production to decrease across the Callovian-Oxfordian boundary, in line with the

geological data, and to explore the geochemical and climatic consequences. However, it should be stressed that the uncertainties about the timing and amplitude of this decrease are large. Consequently, we will test (1) the amplitude and (2) the timing of the neritic carbonate crisis to explore the sensitivity of the Jurassic Earth system to the efficiency of the carbonate factory. The last unknown that will be tested is the relative importance of the neritic production in the total carbonate burial flux prior to the perturbation.

[12] 1. Despite a drastic drawdown in the neritic carbonate production (i.e., reefal and wave-agitated environments), it would be unrealistic to assume a complete cessation of the neritic production. Indeed, patches all around the world of fine-grained carbonate accumulations keep up at a slow rate during the global crisis as evidenced by geological data [Dromart *et al.*, 2003a]. We thus assume that shallow carbonate platform production does not decrease below 20% of its precrisis value. A value of 40% is tested below, and an extreme simulation assuming 0% is also performed.

[13] 2. In line with the geological data, the time span between the collapse of the shallow carbonate platforms from tropical latitudes and the general recovery of shallow carbonate platforms is set to one million years (Figure 1a). This timing is subject to uncertainty. Therefore, we tested the effect of a shorter time span of 100 kyr, thus ten times faster than in the standard case.

[14] 3. Pelagic carbonate production was definitely active at that time but probably restricted to cratonic settings [Opdyke and Wilkinson, 1988]. Indeed, the oldest carbonate pelagic deposits found in ophiolitic complexes and oceanic sequences are (Kimmeridgian)–Tithonian in age, indicating that ante-Tithonian carbonates were mainly deposited over continental cratons [Boss and Wilkinson, 1991]. Using the compilation of carbonate fluxes published by Dromart *et al.* [2003a], we calibrate the model so that about 65% of the total carbonate production occurs as shallow carbonate platforms, and the remaining 35% is supplied by the accumulation of shelfal pelagic carbonate. Because those numbers are subject to uncertainty, we also test the response of the Earth system to cases in which shallow carbonate platforms comprise 85 and 40% of the total carbonate production. The pelagic component is not forced to collapse during the simulation but dynamically responds to changes in the phosphorus supply to the ocean by continental weathering (itself responding to climate change) and to the saturation state of seawater.

[15] For the purpose of discussion, we define a control simulation in which 20% of the shallow carbonate platforms is maintained during the crisis, 65% of the present-day carbonate production occurs on the shallow carbonate platforms prior to the perturbation, and the duration of the crisis lasts one million years.

### 3. Results

#### 3.1. General Case

[16] Salient results of the control simulation are shown in Figure 1. The following analysis holds for all scenarios. First, the disappearance of the midlatitude platforms has almost no effect on atmospheric CO<sub>2</sub> (Figures 1a–1c). This response is due to an increase in the carbonate burial flux on the low-latitude platforms owing to the general increase in the saturation state of the ocean ( $\Omega$ ) (Figure 1c). Indeed, the observed

shutdown of the subtropical platforms drives an imbalance between the weathering fluxes of continental carbonate and silicate and the burial flux of calcium carbonate in sediments, which in turn, leads to an increase in the seawater alkalinity because of Ca<sup>2+</sup> accumulation. The pH of seawater increases, promoting the rise in the CO<sub>3</sub><sup>2-</sup> concentration. On a timescale of 10<sup>4</sup> years, this perturbation is mixed through all basins and leads to an increase in the global saturation state, explaining the increase in burial flux of the tropical platforms that counteracts the rise in alkalinity. Geological support for this scenario comes from stratigraphic data that shows a general encroachment of carbonate platforms onto the low-latitude African-Arabian continent coincident with the decline of the subtropical platforms [Dromart *et al.*, 2003a]. Importantly, the volume-based calculation of carbonate accumulation rates reveals that subtropical decrease of carbonate fluxes is very similar to the increase recorded at lower latitudes [Dromart *et al.*, 2003a]. In a second step, the subsequent shut down of low-latitude platforms has a dramatic effect on seawater chemistry, which in turn, produces an ample decrease in atmospheric CO<sub>2</sub> level in all simulations (Figure 1b). In response to the disappearance of low-latitude carbonate platforms, the atmospheric CO<sub>2</sub> concentration drops from 700 ppmv to 280 ppmv (parts per million by volume). This is because weathering input is only balanced by the shelfal pelagic carbonate burial flux linked to the calcareous nanoplankton producers (Figure 1e). These producers are primarily dependent on the phosphate flux coming from continental weathering [Guidry and Mackenzie, 2000]. Owing to the climatic cooling, phosphorus delivery from the continents decreases inhibiting any increase in pelagic carbonate production. The shutdown of the shallow carbonate platform factory (mainly shallow carbonate platform but also pelagic production) thus leads to an unbalanced increase in calcium concentration. Alkalinity rises readily, increasing the pH of seawater and pushing the carbonate speciation toward the production of CO<sub>3</sub><sup>2-</sup> (Figure 1d). The coeval decrease in H<sub>2</sub>CO<sub>3</sub> promotes the massive dissolution of atmospheric CO<sub>2</sub> into seawater. The fast and continuous drop in CO<sub>2</sub> slows down once the saturation state reaches values greater than 20. Above this value of 20, inorganic physicochemical precipitation occurs in the model [Morse and He, 1993], partly buffering the CO<sub>2</sub> decrease (Figure 1e). One example of abiogenic carbonate deposits during the MLJT is the Upper Jurassic fine-grained limestones in the Western Subalpine Basin [cf. Dromart, 1989]. In this basin, fine-grained limestones of the upper Lower Oxfordian (i.e., Cordatum Zone) are mostly composed of nonskeletal, very fine and well-formed micritic crystals of high-magnesium calcite. The crystals are typically clustered in structureless, rounded, peloidal grains. Such peloidal, or clotted, microfabrics are interpreted to have been microbially originated from supersaturated waters because of their striking microtextural analogy to carbonate deposits of modern highly alkaline environment [e.g., Kazmierczak *et al.*, 1996]. Supporting evidence also comes from the documentation of distal, “deep” waters carbonate stromatolite beds and mud mounds in the Lower Oxfordian of the western Tethys [e.g., Dromart, 1989].

[17] As neritic production is allowed to restart (restoring of the  $F_{\text{down}}$  factor), a short-term warming event is predicted by the model. This occurs because of the highly oversaturated ocean resulting from the brief decrease in the neritic car-



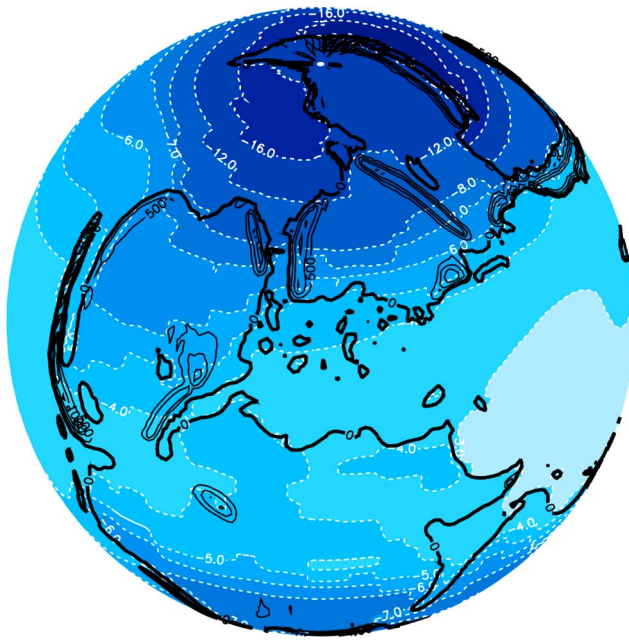


**Figure 3.** Cooling trend through the Middle Late Jurassic transition. Mean annual temperature difference between the low and pre-perturbation partial pressure of  $\text{CO}_2$  described in Figure 1, representing Late Callovian–Early Oxfordian transition and Middle Callovian conditions. An atmospheric  $\text{CO}_2$  level of 700 ppm characterizes Middle Callovian while an atmospheric  $\text{CO}_2$  level of 280 ppm characterizes the MLJT. Black lines show the continental distribution. Stereographic projection centered on the Tethyan area.

bonate production and promoting excess carbonate precipitation relatively to weathering inputs.

### 3.2. Sensitivity Tests

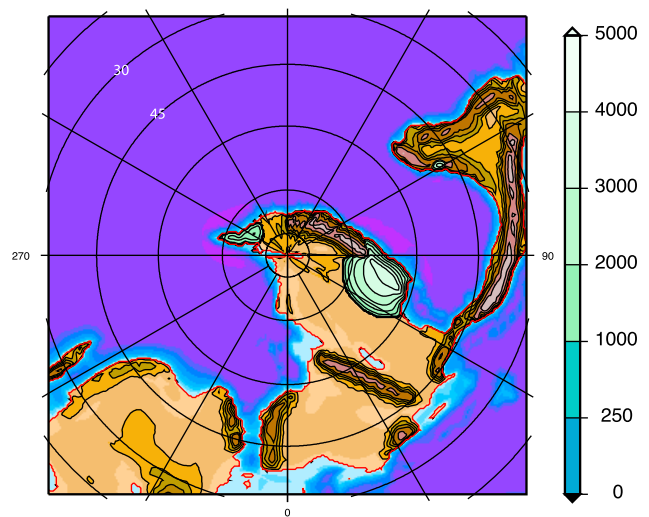
[18] Inherent to any Earth system models applied to deep times, our results are subject to our poor quantitative knowledge of the past environment. In particular, we identify three main parameters for further evaluation: (1) the shallow platform/global carbonate production ratio, (2) the duration of the crisis of the shallow carbonate platforms, and (3) the efficiency of the carbonate production of isolated scattered platforms which survived while the global crisis occurred (Figure 2).

[19] The most important result is that in all sensitivity experiments the model predicts a large drop in atmospheric  $\text{CO}_2$ .  $\text{CO}_2$  falls from 700 ppmv down to values ranging from less than 200 ppmv to 350 ppmv. This  $\text{CO}_2$  drop promotes a global mean temperature decrease of 9.3 and 4.5°C. Increasing the percentage of neritic carbonate production induces a larger decrease of atmospheric  $\text{CO}_2$  although the minimum remains in a narrow range between 300 and 220 ppmv (see black, red and green lines in Figure 2). The duration of the carbonate platform crisis modifies the duration and the amplitude of the cool climatic phase, as well as the survival rate of the platform producers during the crisis. But even in the less favorable case (neritic production accounting for only 40% of the total carbonate burial, survival of 40% of the pre-perturbation neritic production during the crisis, and a fast decline), the impact on the global climate is large. Indeed, the model still predicts a

drawdown of atmospheric  $\text{CO}_2$  to 350 ppmv, which is half the pre-perturbation  $\text{CO}_2$  level (corresponding to a global cooling of 4.5°C). Although 100 kyr is unrealistically short for the Callovian–Oxfordian event, this test illustrates the extreme sensitivity of the Earth system to very short-term collapse of the neritic carbonate production during the ante-Tithonian times. The amplitude of the postcrisis global warming is sensitive to duration of the neritic carbonate crisis. It tends to be low when the crisis is fast because the maximum saturation state with respect to carbonate reached by the seawater during the crisis increases with the duration of the crisis itself. Indeed, when the crisis is assumed to be short (100 kyr), the saturation state of the ocean never reaches the threshold required for abiotic precipitation to start.

[20] Despite the uncertainties related to the reconstruction of the carbonate accumulation flux, we conclude that the

a



b

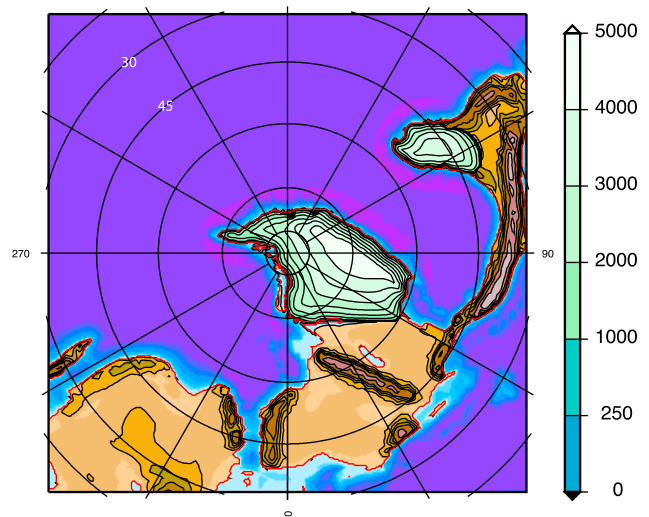
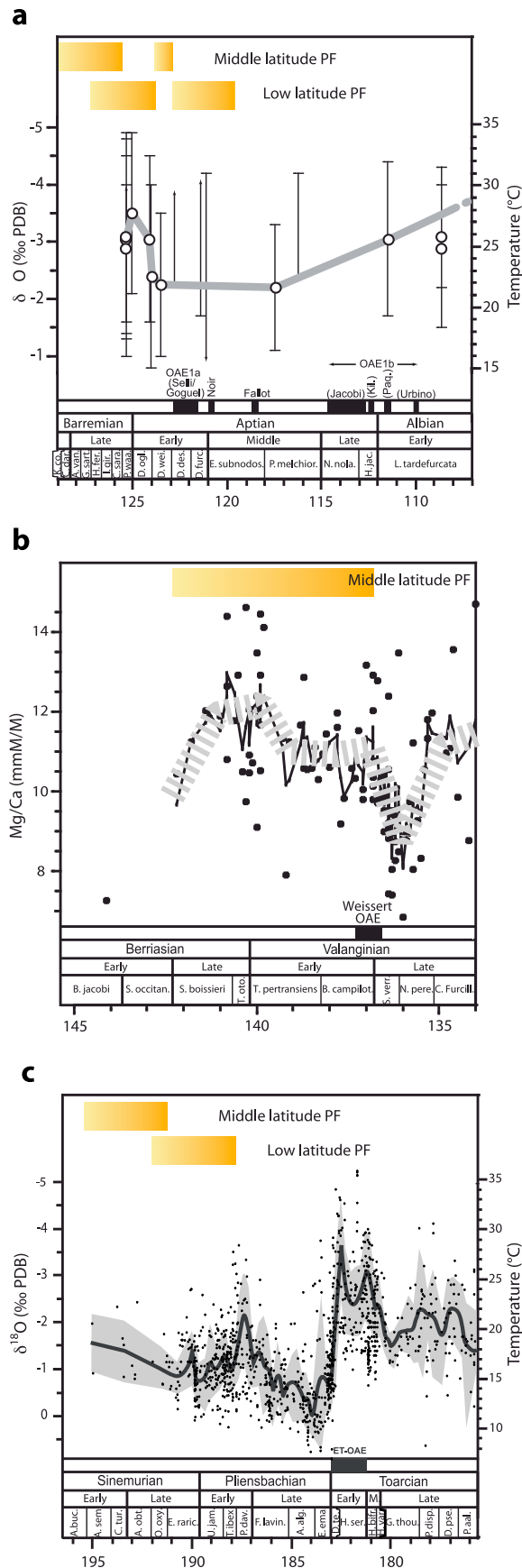


**Figure 4.** Northern polar view of the ice sheet extension through the Middle Late Jurassic transition. (a) Ice sheet topography in meters 70 kyr after the low-latitude carbonate platform collapse. (b) Ice sheet topography in meters 250 kyr after the low-latitude carbonate platform collapse.



carbonate crisis at the MLJT should have had a profound impact on the carbon cycle and climate independent of the scenario adopted.

### 3.3. Comparisons With Data

[21] Our results provide an explanation for triggering a cool event in a globally warm climate. To evaluate how atmospheric  $\text{CO}_2$  change affected surface temperature, we focus on the Tethyan area because the geochemical data sets are biostratigraphically well calibrated, continuous, and ever statistically tested [Dera *et al.*, 2011]. Standard model simulations reproduce a 4°C cooling (Figure 3) from the Middle Callovian to the Callovian-Oxfordian boundary (range of 3–5°C for the whole set of runs), which is consistent with the 4 to 6°C drop recorded by bivalve and belemnite  $\delta^{18}\text{O}$  records from France, England, and Scotland [Anderson *et al.*, 1994; Brigaud *et al.*, 2009; Nunn and Price, 2010]. These estimates are calculated using a constant seawater  $\delta^{18}\text{O}$ , and may be smaller if ice sheets accumulated during this cooling event. Belemnite  $\delta^{18}\text{O}$  data from Poland suggest a smaller but significant decrease of about 2°C [Wierzbowski *et al.*, 2009].

[22] The return of carbonate platforms induces a 6°C warming in our model (range of 5–7°C for the whole set of runs) (not shown). Though a warming trend has been identified during the Early to Middle Oxfordian in the NW Tethyan [Brigaud *et al.*, 2008; Nunn and Price, 2010] and sub-Arctic seas [Price and Rogov, 2009], the amplitude varies from 3 to 8°C depending on the locations and the materials used to measure the  $\delta^{18}\text{O}$ , making it difficult to directly compare our model with data.

[23] Using the modeled temperature and precipitation and imposing modeled  $\text{CO}_2$  changes, we run an offline ice sheet model in order to quantify the extent of the glaciations generated by our scenario (Figure 4). Once  $\text{CO}_2$  goes down to

**Figure 5.** Coevolution of geochemical temperature proxies and carbonate platforms collapse. (a) The Barremian-Aptian. (b) The Berriasian-Valanginian. (c) The Sinemurian-Toarcian. Correspondence between stratigraphic and numerical ages is from Ogg *et al.* [2008]. Geochemical data are from Steuber *et al.* [2005] for Figure 5a, from McArthur *et al.* [2007] for Figure 5b, and from the compilation of Dera *et al.* [2009] for Figure 5c. Data are fitted for Figure 5a using a three-point running mean. For Figure 5a, open circle represent mean annual  $\delta^{18}\text{O}$ , with plain bars corresponding to the range of seasonal variations. Arrows indicate incomplete records of annual minima and/or maxima of  $\delta^{18}\text{O}$  values. For the Jurassic, the greater number of data allows to apply a running average (smoothed black curve) and a standard deviation (gray band) with a bandwidth of 500 kyr. The  $\delta^{18}\text{O}$  values are converted into temperature using the equation of Anderson and Arthur [1981] and a  $\delta^{18}\text{O}$  seawater of −1‰ SMOW. Periods of platform carbonate production crises have been represented by yellow to brown horizontal bars [Dromart *et al.*, 1996; Föllmi *et al.*, 1994, 2006; Lachkar *et al.*, 2009; Morettini *et al.*, 2002; Quesada *et al.*, 2005; Rousseau *et al.*, 2005; Ruiz-Ortiz *et al.*, 2004; van Buchem *et al.*, 2002; Weissert *et al.*, 1998]. Note that the proposed reconstructions of the carbonate crisis are tentative and clearly not definitive. The occurrence of oceanic anoxic events (OAE) has been reported for all periods [Dromart *et al.*, 2003a; Erba *et al.*, 2004; Jenkyns, 1988; Quesada *et al.*, 2005].

400 ppmv, small ice caps form on the highest elevations of the Siberia craton, and on the North China craton and spreads to lowlands when lower CO<sub>2</sub> occur (below 300 ppmv). There is no continental ice formation in the Southern Hemisphere in our model. We also translate the simulated ice volume into sea level changes. On the basis of our sensitivity runs, we predict a sea level drop ranging from 14 to 62 m (Figure 2b). Our predicted range of sea level drop is in agreement with estimates of several tens of meters inferred from depositional facies analysis in Iberian Peninsula [Dromart *et al.*, 2003b]. In details, Dromart *et al.* [2003b] have reviewed a variety of sedimentological evidence that may indicate a sea level drop around the MLJT (i.e., basin fans in deep waters, bypass and ravinement on shelves); however, no direct evidence for continental ice has been found for this time period.

#### 4. Discussion

[24] Shallow-water biotic communities respond closely to environmental changes, and several factors can induce carbonate platform demise. These communities are sensitive to changes in sea level, detrital influx rates and nutrient levels, wave and current energy, water temperature, storm events, and various tectonic processes, among others [Föllmi *et al.*, 1994]. The origin of the platform demise of the Callovian-Oxfordian period remains unclear. Here we speculate on some scenarios.

[25] The climatic deterioration initiated in our model by the carbonate production crisis in low-latitude regions may exert a feedback on carbonate production: cooler conditions may further promote neritic carbonate decline by shrinking the latitudinal extension of carbonate platforms. Such a process would introduce a positive feedback loop that is only interrupted by the onset of abiotic carbonate deposition, which removes alkalinity from the ocean and counteracts the massive atmospheric CO<sub>2</sub> dissolution in seawater. In our model, the onset of abiotic carbonate production causes carbon to degas from the ocean into the atmosphere as alkalinity decreases again. Hence, temperature rises before the crisis ends, possibly allowing neritic producers to settle again, further helped by the high saturation index of the seawater. The link between the available neritic area and the sea level may also be a candidate. Similarly, an initial sea level decrease may reduce the space for shallow carbonate platforms and induce a decrease of carbonate production, which in turn, should cool the climate and further decrease the sea level. There is therefore the potential in such a system for generating short-lived ice ages from only a small initial perturbation. Nevertheless, at least in our model, ice sheets appear after the demise of the tropical shallow carbonate platforms rendering such a positive feedback inefficient. It should still be recognized that this feedback loop might be efficient if the CO<sub>2</sub> threshold below which ice sheets begin to form was higher. This threshold remains model-dependent and may change from one continental configuration to another. The initiation of ice sheets is also very sensitive to topography, continental geometry, orbital parameters, and other factors [Horton *et al.*, 2010].

[26] Independent of the initial trigger of the carbonate production crisis, we show that this demise will result in an additional cooling and in a limited ice sheet build up. The quantification holds against the uncertainties inherent to our

model and the sea level drawdown is in agreement with data. Carbonate platform drawdown may explain other cooling episodes recorded during the Mesozoic [Föllmi *et al.*, 2006; van Buchem *et al.*, 2002; Weissert *et al.*, 1998]. Figure 5 presents available records of geochemical temperature proxies for three additional periods that recorded short-term cooling events and the occurrence of shallow carbonate platform crises. Additional data are still needed to accurately constrain the timing of these cooling events, especially for the Barremian-Aptian period, and very few information are available on the behavior of tropical shallow carbonate platforms during the Berriasian-Valanginian. However, according to the data currently available, all these episodes seem to be preceded by the drowning or exposure of subtropical shallow carbonate platforms, and by the beginning of tropical shallow carbonate platforms demise. Low-latitude carbonate platform crises seem to occur slightly before or during the cooling trend as it happens in our scenario (Figure 1).

[27] Other processes may have contributed to the occurrence of these cooling events [Weissert and Erba, 2004], like extensive organic carbon burial during oceanic anoxic events (OAEs) that is not considered in our model. More modeling studies are required to decipher the respective roles of the carbonate platforms demise and of the onset of OAEs on climate. We hope to improve our understanding of these issues in the near future using a new version of GEOCLIM called GEOCLIM reloaded that will integrate processes linked to ocean anoxia and organic carbon storage in sediments [Arndt *et al.*, 2011].

#### 5. Conclusions

[28] Our model results provide a geologically based explanation for the severe cooling observed during the MLJT, and highlight the complex control of carbonate accumulation pattern on a Myr timescale. Our model results do provide a quantified mechanism to explain these cool events, shedding light on the high sensitivity of the Earth system to perturbations in carbonate system deposition. With the implementation of an ice sheet model, we also provide ranges of sea level fall induced by the decrease in atmospheric CO<sub>2</sub> in agreement with the magnitude of sea level change inferred from sedimentological data. As a concluding remark, it is interesting to note that such cool episodes on the Myr timescale disappear after the Cretaceous which may be a consequence of the development of an extended and responsive deep-sea carbonate sinks [Ridgwell *et al.*, 2003].

[29] **Acknowledgments.** This work has been motivated by the interdisciplinary program ECLIPSE-2 (INSU-CNRS). We acknowledge C. Poulsen, G. Price, K. Föllmi, and one anonymous reviewer for their constructive comments that have greatly helped to improve this manuscript.

#### References

- Abbink, O. A., J. Targarona, H. Brinkhuis, and H. Visscher (2001), Late Jurassic to earliest Cretaceous palaeoclimatic evolution of the southern North Sea, *Global Planet. Change*, 30, 231–256, doi:10.1016/S0921-8181(01)00101-1.
- Anderson, T. F., and M. A. Arthur (1981), Stable isotopes of oxygen and carbon and their application to sedimentologic and paleoenvironmental problems, in *Stable Isotopes in Sedimentary Geology*, edited by M. A. Arthur *et al.*, pp. 1–151, Soc. for Sediment. Geol., Tulsa, Okla.



- Anderson, T. F., B. N. Popp, A. C. Williams, L. Z. Ho, and J. D. Hudson (1994), The stable isotopic records of fossils from the Peterborough Member, Oxford Clay Formation (Jurassic), UK: Palaeoenvironmental implication, *J. Geol. Soc.*, **151**, 125–138.
- Arndt, S., P. Regnier, Y. Godd  ris, and Y. Donnadieu (2011), GEOCLIM reloaded (v 1.0): A new coupled Earth system model for past climate change, *Geosci. Model Dev.*, **4**, 451–481.
- Berner, R. A. (1997), The rise of plants and their effect on weathering and atmospheric CO<sub>2</sub>, *Science*, **276**, 544–546, doi:10.1126/science.276.5312.544.
- Besse, J., and V. Courtillot (2002), Apparent and true polar wander and the geometry of the geomagnetic field over the last 200 Myr, *J. Geophys. Res.*, **107**(B11), 2300, doi:10.1029/2000JB000050.
- Boss, S. K., and B. H. Wilkinson (1991), Planktonic eustatic control on cratonic oceanic carbonate accumulation, *J. Geol.*, **99**(4), 497–513, doi:10.1086/629513.
- Brigaud, B., et al. (2008), Climatic fluctuations and seasonality during the Late Jurassic (Oxfordian–Early Kimmeridgian) inferred from  $\delta^{18}\text{O}$  of Paris Basin oyster shells, *Earth Planet. Sci. Lett.*, **273**, 58–67, doi:10.1016/j.epsl.2008.06.015.
- Brigaud, B., et al. (2009), Facies and climate/environmental changes recorded on a carbonate ramp: A sedimentological and geochemical approach on Middle Jurassic carbonates (Paris Basin, France), *Sediment. Geol.*, **222**(3–4), 181–206, doi:10.1016/j.sedgeo.2009.09.005.
- Caldeira, K., and M. R. Rampino (1993), Aftermath of the end-Cretaceous mass extinction: Possible biogeochemical stabilization of the carbon cycle and climate, *Paleoceanography*, **8**, 515–525, doi:10.1029/93PA01163.
- Catubig, N. R., D. E. Archer, R. Francois, P. deMenocal, W. Howard, and E.-F. Yu (1998), Global deep-sea burial rate of calcium carbonate during the Last Glacial Maximum, *Paleoceanography*, **13**, 298–310, doi:10.1029/98PA00609.
- Coxall, H. K., et al. (2005), Rapid stepwise onset of Antarctic glaciation and deeper calcite compensation in the Pacific Ocean, *Nature*, **433**, 53–57, doi:10.1038/nature03135.
- DeConto, R., and D. Pollard (2003), Rapid Cenozoic glaciation of Antarctica induced by declining atmospheric CO<sub>2</sub>, *Nature*, **421**, 245–249, doi:10.1038/nature01290.
- Dera, G., E. Puc  at, P. Pellenard, P. Neige, D. Delsate, M. M. Joachimski, L. Reisberg, and M. Martinez (2009), Water mass exchange and variations in seawater temperature in the NW Tethys during the Early Jurassic: Evidence from neodymium and oxygen isotopes of fish teeth and belemnites, *Earth Planet. Sci. Lett.*, **286**, 198–207, doi:10.1016/j.epsl.2009.06.027.
- Dera, G., et al. (2011), Climatic ups and downs in a disturbed Jurassic world, *Geology*, **39**, 215–218, doi:10.1130/G31579.1.
- Dercourt, J., L. E. Ricou, and B. Vrielynck (1993), *Atlas Tethys Palaeoenvironmental Maps: Explanatory Notes*, 307 pp., Gauthier-Villars, Paris.
- Donnadieu, Y., et al. (2004), A “snowball Earth” climate triggered by continental break-up through changes in runoff, *Nature*, **428**, 303–306, doi:10.1038/nature02408.
- Donnadieu, Y., Y. Godd  ris, R. Pierrehumbert, G. Dromart, F. Fluteau, and R. Jacob (2006), A GEOCLIM simulation of climatic and biogeochemical consequences of Pangea breakup, *Geochem. Geophys. Geosyst.*, **7**, Q11019, doi:10.1029/2006GC001278.
- Donnadieu, Y., et al. (2009), Exploring the climatic impact of the continental vegetation on the Mesozoic atmospheric CO<sub>2</sub> and climate history, *Clim. Past*, **5**(1), 85–96, doi:10.5194/cp-5-85-2009.
- Dromart, G. (1989), Deposition of Upper Jurassic fine-grained limestones in the western subalpine basin, France, *Palaeogeogr. Palaeoclimatol. Palaeoecol.*, **69**, 23–43, doi:10.1016/0031-0182(89)90154-5.
- Dromart, G., et al. (1996), Variation cyclique de la production carbonat  e au Jurassique le long d’un transect Bourgogne-Ard  che, Est-France, *Bull. Soc. Geol. Fr.*, **167**, 423–433.
- Dromart, G., et al. (2003a), Perturbation of the carbon cycle at the Middle/Late Jurassic transition: Geological and geochemical evidence, *Am. J. Sci.*, **303**, 667–707, doi:10.2475/ajs.303.8.667.
- Dromart, G., et al. (2003b), Ice age at the Middle-Late Jurassic transition?, *Earth Planet. Sci. Lett.*, **213**, 205–220, doi:10.1016/S0012-821X(03)00287-5.
- Erba, E., et al. (2004), Valanginian Weissert oceanic anoxic event, *Geology*, **32**, 149–152, doi:10.1130/G20008.1.
- F  llmi, K. B., H. Weissert, M. Bisping, and H. Funk (1994), Phosphogenesis, carbon-isotope stratigraphy, and carbonate-platform evolution along the Lower Cretaceous northern Tethyan Margin, *Geol. Soc. Am. Bull.*, **106**(6), 729–746, doi:10.1130/0016-7606(1994)106<0729:PCISAC>2.3.CO;2.
- F  llmi, K. B., A. Godet, S. Bodin, and P. Linder (2006), Interactions between environmental change and shallow water carbonate buildup along the northern Tethyan margin and their impact on the Early Cretaceous carbon isotope record, *Paleoceanography*, **21**, PA4211, doi:10.1029/2006PA001313.
- Gaillardet, J., et al. (1999), Global silicate weathering and CO<sub>2</sub> consumption rates deduced from the chemistry of the large rivers, *Chem. Geol.*, **159**, 3–30, doi:10.1016/S0009-2541(99)00031-5.
- Gehlen, M., et al. (2007), The fate of pelagic CaCO<sub>3</sub> production in a high CO<sub>2</sub> ocean: A model study, *Biogeosciences*, **4**(4), 505–519, doi:10.5194/bg-4-505-2007.
- Godderis, Y., and M. M. Joachimski (2004), Global change in the Late Devonian: Modelling the Frasnian–Famennian short-term carbon isotope excursions, *Palaeogeogr. Palaeoclimatol. Palaeoecol.*, **202**, 309–329.
- Godderis, Y., et al. (2008), Causal or casual link between the rise of nanoplankton calcification and a tectonically driven massive decrease in Late Triassic atmospheric CO<sub>2</sub>?, *Earth Planet. Sci. Lett.*, **267**, 247–255, doi:10.1016/j.epsl.2007.11.051.
- Gough, D. O. (1981), Solar interior structure and luminosity variations, *Sol. Phys.*, **74**, 21–34.
- Guidry, M. W., and F. T. Mackenzie (2000), Apatite weathering and the Phanerozoic phosphorus cycle, *Geology*, **28**, 631–634, doi:10.1130/0091-7613(2000)28<631:AWATPP>2.0.CO;2.
- Hoffman, P. F., et al. (1998), A Neoproterozoic snowball Earth, *Science*, **281**, 1342–1346, doi:10.1126/science.281.5381.1342.
- Horton, D. E., C. J. Poulsen, and D. Pollard (2007), Orbital and CO<sub>2</sub> forcing of late Paleozoic continental ice sheets, *Geophys. Res. Lett.*, **34**, L19708, doi:10.1029/2007GL031188.
- Horton, D. E., et al. (2010), Influence of high-latitude vegetation feedbacks on late Paleozoic glacial cycles, *Nat. Geosci.*, **3**, 572–577, doi:10.1038/ngeo922.
- Jenkyns, H. C. (1988), The Early Toarcian (Jurassic) anoxic event: Stratigraphic, sedimentary, and geochemical evidence, *Am. J. Sci.*, **288**, 101–151, doi:10.2475/ajs.288.2.101.
- Kazmierczak, J., et al. (1996), Cyanobacterial key to the genesis of micritic and peloidal limestones in ancient seas, *Acta Palaeontol. Pol.*, **41**, 319–338.
- Kiessling, W. (2001), Paleoclimatic significance of Phanerozoic reefs, *Geology*, **29**, 751–754, doi:10.1130/0091-7613(2001)029<0751:PSOPR>2.0.CO;2.
- Lachkar, N., et al. (2009), Early Jurassic normal faulting in a carbonate extensional basin: Characterization of tectonically driven platform drowning (High Atlas rift, Morocco), *J. Geol. Soc.*, **166**, 413–430, doi:10.1144/0016-76492008-084.
- MacAyeal, D. R. (1989), Large-scale ice flow over a viscous basal sediment: Theory and application to ice stream B, Antarctica, *J. Geophys. Res.*, **94**, 4071–4087, doi:10.1029/JB094iB04p04071.
- McArthur, J. M., et al. (2007), Palaeotemperatures, polar ice-volume, and isotope stratigraphy (Mg/Ca,  $\delta^{18}\text{O}$ ,  $\delta^{13}\text{C}$ ,  $^{87}\text{Sr}/^{86}\text{Sr}$ ), The Early Cretaceous (Berriasian, Valanginian, Hauterivian), *Palaeogeogr. Palaeoclimatol. Palaeoecol.*, **248**, 391–430, doi:10.1016/j.palaeo.2006.12.015.
- Meric  , A., et al. (2008), Eocene/Oligocene ocean de-acidification linked to Antarctic glaciation by sea-level fall, *Nature*, **452**, 979–982, doi:10.1038/nature06853.
- Moretini, E., et al. (2002), Carbon isotope stratigraphy and carbonate production during the Early Middle Jurassic: Examples from the Umbria–Marche–Sabina Apennines (central Italy), *Palaeogeogr. Palaeoclimatol. Palaeoecol.*, **184**, 251–273, doi:10.1016/S0031-0182(02)00258-4.
- Morse, J. W., and S. He (1993), Influences of T, S and pCO<sub>2</sub> on the pseudo-homogeneous precipitation of CaCO<sub>3</sub> from seawater: Implications for whiting formation, *Mar. Chem.*, **41**, 291–297, doi:10.1016/0304-4203(93)90261-L.
- Nunn, E., and G. Price (2010), Late Jurassic (Kimmeridgian–Tithonian) stable isotopes ( $\delta^{18}\text{O}$  and  $\delta^{13}\text{C}$ ) and Mg/Ca ratios: New palaeoclimate data from Helmsdale, northeast Scotland, *Palaeogeogr. Palaeoclimatol. Palaeoecol.*, **292**, 325–335, doi:10.1016/j.palaeo.2010.04.015.
- Ogg, J. G., et al. (2008), *The Concise Geologic Time Scale*, Cambridge Univ. Press, Cambridge, U. K.
- Opdyke, B. N., and B. H. Wilkinson (1988), Surface area control of shallow cratonic to deep marine carbonate accumulation, *Paleoceanography*, **3**, 685–703, doi:10.1029/PA003i006p00685.
- Orr, J. C., et al. (2005), Anthropogenic ocean acidification over the twenty-first century and its impact on calcifying organisms, *Nature*, **437**, 681–686, doi:10.1038/nature04095.
- Pellenard, P., and J.-F. Deconinck (2006), Mineralogical variability of Callovo–Oxfordian clays from the Paris Basin and the Subalpine Basin, *C. R. Geosci.*, **338**, 854–866, doi:10.1016/j.crte.2006.05.008.
- Price, G., and M. Rogov (2009), An isotopic appraisal of the Late Jurassic greenhouse phase in the Russian Platform, *Palaeogeogr. Palaeoclimatol. Palaeoecol.*, **273**, 41–49, doi:10.1016/j.palaeo.2008.11.011.
- Quesada, S., et al. (2005), Depositional architecture and transgressive-regressive cycles within Liassic backstepping carbonate ramps in the Basque Cantabrian basin, northern Spain, *J. Geol. Soc.*, **162**, 531–548, doi:10.1144/0016-764903-041.

- Ridgwell, A. J., et al. (2003), Carbonate deposition, climate stability, and Neoproterozoic ice ages, *Science*, *302*, 859–862, doi:10.1126/science.1088342.
- Ritz, C., V. Rommelaere, and C. Dumas (2001), Modeling the evolution of Antarctic ice sheet over the last 420,000 years: Implications for altitude changes in the Vostok region, *J. Geophys. Res.*, *106*, 31,943–31,964, doi:10.1029/2001JD900232.
- Rousseau, M., et al. (2005), Jurassic evolution of the Arabian carbonate platform edge in the central Oman Mountains, *J. Geol. Soc.*, *162*, 349–362, doi:10.1144/0016-764903-178.
- Royer, D. L., et al. (2004), CO<sub>2</sub> as a primary driver of Phanerozoic climate, *GSA Today*, *14*, 4–10, doi:10.1130/1052-5173(2004)014<4:CAAPDO>2.0.CO;2.
- Ruiz-Ortiz, P. A., et al. (2004), Tectonic control of facies architecture, sequence stratigraphy and drowning of a Liassic carbonate platform (Betic Cordillera, southern Spain), *Basin Res.*, *16*, 235–257, doi:10.1111/j.1365-2117.2004.00231.x.
- Steuber, T., et al. (2005), Low-latitude seasonality of Cretaceous temperatures in warm and cold episodes, *Nature*, *437*, 1341–1344, doi:10.1038/nature04096.
- Thierry, J., et al. (2006), The Callovian–Oxfordian ammonites of the ANDRA bore-holes of the eastern Paris Basin: Biochronostratigraphic synthesis, palaeoecological and palaeobiogeographical interests, *C. R. Geosci.*, *338*, 834–853, doi:10.1016/j.crte.2006.05.005.
- van Buchem, F., et al. (2002), High resolution sequence stratigraphic architecture of Barremian/Aptian carbonate systems in northern Oman and the United Arab Emirates, *GeoArabia*, *7*, 461–500.
- Walker, J. C. G., P. B. Hays, and J. F. Kasting (1981), A negative feedback mechanism for the long-term stabilization of Earth's surface temperature, *J. Geophys. Res.*, *86*, 9776–9782, doi:10.1029/JC086iC10p09776.
- Weissert, H., and E. Erba (2004), Volcanism, CO<sub>2</sub> and palaeoclimate: A Late Jurassic–Early Cretaceous carbon and oxygen isotope record, *J. Geol. Soc.*, *161*, 695–702, doi:10.1144/0016-764903-087.
- Weissert, H., et al. (1998), Correlation of Early Cretaceous carbon isotope stratigraphy and platform drowning events: A possible link?, *Palaeogeogr. Palaeoclimatol. Palaeoecol.*, *137*, 189–203, doi:10.1016/S0031-0182(97)00109-0.
- Wierzbowski, H., and M. Rogov (2011), Reconstructing the palaeoenvironment of the Middle Russian Sea during the Middle–Late Jurassic transition using stable isotope ratios of Cephalopod shells and variations in faunal assemblages, *Palaeogeogr. Palaeoclimatol. Palaeoecol.*, *299*, 250–264, doi:10.1016/j.palaeo.2010.11.006.
- Wierzbowski, H., K. Dembicz, and T. Praszkiel (2009), Oxygen and carbon isotope composition of Callovian–Lower Oxfordian (Middle–Upper Jurassic) belemnite rostra from central Poland: A record of a Late Callovian global sea-level rise?, *Palaeogeogr. Palaeoclimatol. Palaeoecol.*, *283*, 182–194.

B. Brigaud, UMR 8148, Université Paris-Sud 11, CNRS, F-91405 Orsay, France.

G. Dera, Y. Donnadieu, and C. Dumas, LSCE, IPSL, CEA-CNRS-UVSQ, F-91191 Gif-sur-Yvette, France. (yannick.donnadieu@lsce.ipsl.fr)

G. Dromart and N. Olivier, UMR 5570, Université de Lyon, CNRS, ENS de Lyon, F-69364 Lyon, France.

Y. Goddérès, LMTG, CNRS-Université Paul Sabatier, F-31400 Toulouse, France.

E. Pucéat, Université de Bourgogne, CNRS, Biogéosciences, F-2100 Dijon, France.